32ND INTERNATIONAL COSMIC RAY CONFERENCE, BEIJING 2011

A study of the mass composition of cosmic rays based on an event-by-event assignment with KASCADE-Grande data

M. BERTAINA[1], W.D. APEL[2], J.C. ARTEAGA-VELÁZQUEZ[3], K. BEKK[2], J. BLÜMER[2,4], H. BOZDOG[2], I.M. BRANCUS[5], P. BUCHHOLZ[6], E. CANTONI[1,7], A. CHIAVASSA[1], F. COSSAVELLA[4,13], K. DAUMILLER[2], V. DE SOUZA[8], F. DI PIERRO[1], P. DOLL[2], R. ENGEL[2], J. ENGLER[2], M. FINGER[4], D. FUHRMANN[9], P.L. GHIA[7], H.J. GILS[2], R. GLASSTETTER[9], C. GRUPEN[6], A. HAUNGS[2], D. HECK[2], J.R. HÖRANDEL[10], D. HUBER[4], T. HUEGE[2], P.G. ISAR[2,14], K.-H. KAMPERT[9], D. KANG[4], H.O. KLAGES[2], K. LINK[4], P. ŁUCZAK[11], M. LUDWIG[4], H.J. MATHES[2], H.J. MAYER[2], M. MELISSAS[4], J. MILKE[2], B. MITRICA[5], C. MORELLO[7], G. NAVARRA[1,15], J. OEHLSCHLÄGER[2], S. OSTAPCHENKO[2,16], S. OVER[6], N. PALMIERI[4], M. PETCU[5], T. PIEROG[2], H. REBEL[2], M. ROTH[2], H. SCHIELER[2], F.G. SCHRÖDER[2], O. SIMA[12], G. TOMA[5], G.C. TRINCHERO[7], H. ULRICH[2], A. WEINDL[2], J. WOCHELE[2], M. WOMMER[2], J. ZABIEROWSKI[11]

[1] *Dipartimento di Fisica Generale dell' Università Torino, Italy*
[2] *Institut für Kernphysik, KIT - Karlsruher Institut für Technologie, Germany*
[3] *Universidad Michoacana, Instituto de Física y Matemáticas, Morelia, Mexico*
[4] *Institut für Experimentelle Kernphysik, KIT - Karlsruher Institut für Technologie, Germany*
[5] *National Institute of Physics and Nuclear Engineering, Bucharest, Romania*
[6] *Fachbereich Physik, Universität Siegen, Germany*
[7] *Istituto di Fisica dello Spazio Interplanetario, INAF Torino, Italy*
[8] *Universidade São Paulo, Instituto de Física de São Carlos, Brasil*
[9] *Fachbereich Physik, Universität Wuppertal, Germany*
[10] *Dept. of Astrophysics, Radboud University Nijmegen, The Netherlands*
[11] *Soltan Institute for Nuclear Studies, Lodz, Poland*
[12] *Department of Physics, University of Bucharest, Bucharest, Romania*
[13] *now at: Max-Planck-Institut Physik, München, Germany;* [14] *now at: Institute Space Sciences, Bucharest, Romania;* [15] *deceased;* [16] *now at: Univ Trondheim, Norway*
bertaina@to.infn.it

DOI: 10.7529/ICRC2011/V01/0312

Abstract: The cosmic ray energy spectrum between 10^{16} eV and 10^{18} eV is reconstructed in KASCADE-Grande by correlating the size of the charged particles (N_{ch}) and muons (N_μ) on an event-by-event basis. In the energy assignment, the mass sensitivity is minimized by means of a parameter $k(N_{ch}, N_\mu)$. On the other hand, the evolution of k as a function of energy keeps track of the evolution of the composition, and allows an event-by-event separation between electron rich and electron poor primaries. A first result on the evolution of k and its connection with the shape of the energy spectrum, is presented in the framework of the QGSJet II-03 interaction model.

Keywords: Composition, energy spectrum, 10^{16} - 10^{18} eV, KASCADE-Grande.

1 Introduction

The study of the energy spectrum and of the chemical composition of cosmic rays are fundamental tools to understand origin, acceleration and propagation of cosmic rays. The energy range between 10^{16} eV and 10^{18} eV is quite important from astrophysical point of view because it is expected that in this energy range the transition between galactic and extra-galactic origin of cosmic rays will occur. The results obtained at lower energies by KASCADE [1] and EAS-TOP [2] as well as by other experiments suggest that the knee in the primary energy spectrum around 3 - 4 $\times$ 10^{15} eV is due to the break in the spectra of light elements. Moreover, KASCADE results seem to indicate that a rigidity dependent mechanism is responsible for such knees. Therefore, a knee of the heaviest components would be expected in the range of 10^{16} eV to 10^{18} eV. Various theories with different assumptions try to explain the rather smooth behavior of the cosmic ray energy spectrum in this energy range (i.e. [3, 4]). In order to discriminate between the different models, a very precise measurement of the possible structures of the energy spectrum and of the evolution of the composition is needed.

2 The Technique

The technique employed to derive the all-particle energy spectrum and the abundance of electron-rich (e.r.) and electron-poor (e.p.) primaries is based on the correlation between the size of the charged particles (N_{ch}) and muons (N_μ) on an event-by-event basis. The method itself has been described in detail in [5].

A sample of Monte Carlo data was simulated including the full air shower development in the atmosphere, the response of the detector and its electronics as well as their uncertainties. In this way, the parameters reconstructed from simulation are obtained in the same way as for real data. The EAS events were generated with an isotropic distribution with spectral index $\gamma = -3$ and were simulated with CORSIKA [6] and the hadronic Monte Carlo generators FLUKA [7] and QGSJet II-03 [8]. Sets of simulated events were produced in the energy range from 10^{15} eV to 10^{18} eV with high statistics and for five elements: H, He, C, Si and Fe, representative for different mass groups (≈ 353.000 events per primary). Few events up to $3 \cdot 10^{18}$ eV were also generated in order to cross-check the reconstruction behavior at the highest energies.

Grande stations [9] are used to provide core position and angle-of-incidence, as well as the total number of charged particles in the shower, by means of a maximum likelihood procedure comparing the measured number of particles with the one expected from a modified NKG lateral distribution function [10] of charged particles in the EAS.

The total number of muons is calculated using the core position determined by the Grande array and the muon densities measured by the KASCADE muon array detectors. The total number of muons N_μ in the shower disk (above the energy threshold of 230 MeV) is derived from a maximum likelihood estimation assuming a lateral distribution function based on the one proposed by Lagutin and Raikin [11]. The reconstruction procedures and obtained accuracies of KASCADE-Grande observables are described in detail in reference [9].

For the reconstructed events, we restricted ourselves to events with zenith angles lower than $40°$. Additionally, only air showers with cores located in a central area on KASCADE-Grande were selected. With this cut on the fiducial area, border effects are discarded and possible under- and overestimations of the muon number for events close to and far away from the center of the KASCADE array are reduced. All of these cuts were applied also to the Monte Carlo simulations to study the effects and to optimize the cuts. Full efficiency for triggering and reconstruction of air-showers is reached at primary energy of $\approx 10^{16}$eV, slightly depending on the cuts needed for the reconstruction of the different observables [9].

The analysis presented here is finally based on 1173 days of data and the cuts on the sensitive central area and zenith angle correspond to a total acceptance of $A = 1.976 \cdot 10^9$ cm$^2\cdot$ sr, and an exposure of $N = 2.003 \cdot 10^{17}$ cm$^2\cdot$ s·sr, respectively.

With Monte Carlo simulations a formula is obtained to calculate the primary energy per individual shower on the basis of N_{ch} and N_μ. The formula takes into account the mass sensitivity in order to minimize the composition dependence in the energy assignment, and at the same time, provides an event-by-event separation between e.r. and e.p. candidates. The formula is defined for 5 different zenith angle intervals ($\theta < 16.7$, $16.7 \leq \theta < 24.0$, $24.0 \leq \theta < 29.9$, $29.9 \leq \theta < 35.1$, $35.1 \leq \theta < 40.0$) independently, to take into account the shower attenuation in atmosphere. Data are combined only at the very last stage to obtain a unique power law spectrum and mass composition. The energy assignment is defined as $E = f(N_{ch}, k)$ (see equation 1), where N_{ch} is the size of the charged particle component and the parameter k is defined through the ratio of the sizes of the N_{ch} and muon (N_μ) components: $k = g(N_{ch}, N_\mu)$ (see equation 2). The main aim of the k variable is to take into account the average differences in the N_{ch}/N_μ ratio among different primaries with same N_{ch} and the shower to

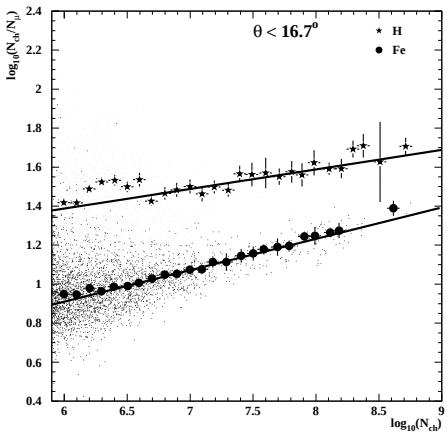

Figure 1: Scatter plot of the reconstructed N_{ch}/N_μ vs. N_{ch} for H and Fe primaries for the first angular bin. The full dots and error bars indicate the mean and its statistical error of the distribution of the individual events (small dots). The fits result in parameters c and d of expression 3.

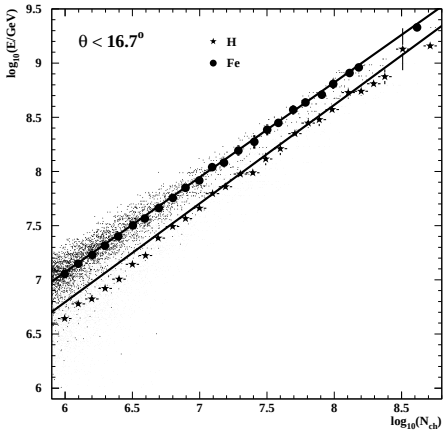

Figure 2: Scatter plot of E vs. N_{ch} for Fe and H primaries. The fits result in parameters a and b of expression 1.

Table 1: Parameters of the calibration functions.

Angles[deg]	a		b		c		d	
	H	Fe	H	Fe	H	Fe	H	Fe
$0.0 - 16.7$	0.910	0.876	1.333	1.817	0.100	0.161	0.786	-0.055
$16.7 - 24.0$	0.894	0.878	1.495	1.923	0.081	0.179	0.884	-0.254
$24.0 - 29.9$	0.937	0.889	1.301	1.935	0.104	0.156	0.677	-0.170
$29.9 - 35.1$	0.934	0.881	1.458	2.099	0.109	0.171	0.543	-0.351
$35.1 - 40.0$	0.919	0.875	1.748	2.287	0.105	0.156	0.412	-0.348

shower fluctuations for events of the same primary mass:

$$log_{10}(E[GeV]) = [a_H + (a_{Fe} - a_H) \cdot k] \cdot log_{10}(N_{ch}) + + b_H + (b_{Fe} - b_H) \cdot k \quad (1)$$

$$k = \frac{log_{10}(N_{ch}/N_\mu) - log_{10}(N_{ch}/N_\mu)_H}{log_{10}(N_{ch}/N_\mu)_{Fe} - log_{10}(N_{ch}/N_\mu)_H} \quad (2)$$

$$log_{10}(N_{ch}/N_\mu)_{H,Fe} = c_{H,Fe} \cdot log_{10}(N_{ch}) + d_{H,Fe}. \quad (3)$$

The k parameter is, by definition of eq. (2), a number centered around 0 for H showers and 1 for Fe ones if expressed as a function of N_{ch}, while slightly shifted when reported as a function of energy (see Fig. 4). The complete list of parameters a -d can be found in table 1.

Figs. 1, 2 show the scatter plots with the parametrizations

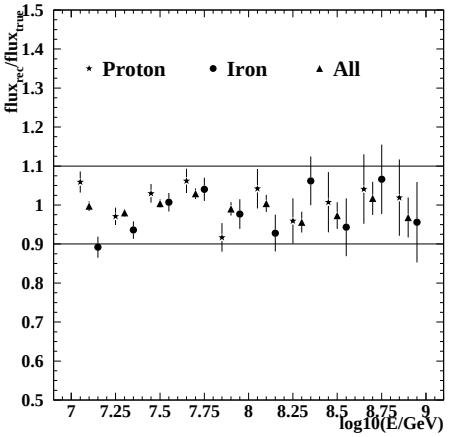

Figure 3: Ratio between the reconstructed and true simulated energy spectra for H, Fe and all mixed primaries summing up all angular bins.

defined for H and Fe in the first angular bin, while Fig. 3 shows the capability of reproducing simulated energy spectra. Pure spectra of H, Fe and a mixture of 5 different primaries with 20% abundance each are shown as examples. The true flux is always reproduced within 10% uncertainty.

3 Results

Fig. 4 shows, for the sum of the first two angular bins, the evolution of the k parameter as a function of the reconstructed energy obtained by simulating with QGSJet II-03 model pure H, He, C, Si, Fe primary spectra, as well as for the experimental data. Similar behavior is obtained also for the other angular bins. The error bars indicate the average

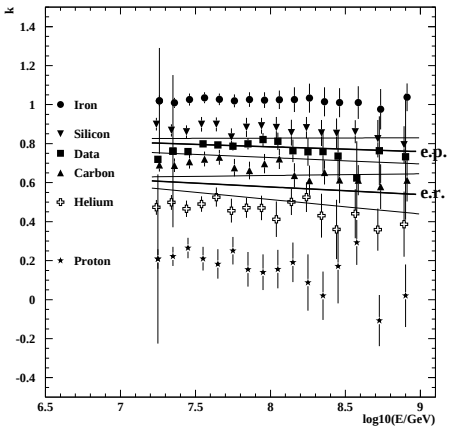

Figure 4: Evolution of the k parameter as a function of the reconstructed energy for experimental data compared with pure primary spectra for the angular range 0-24°. The error bars assign statistical as well as recostruction uncertainties of k.

dispersion of the k parameter among different bins, which include statistical errors, and systematic uncertainty of equations 3 in each angular bin. Fig. 4 shows also two thick straight lines which are used to classify events into different mass groups. The classification is done for each angular bin, independently, to avoid possible systematic effects among the bins. The top thick line represents the separation between e.p. and intermediate samples and it is defined by fitting the $k_{e.p.}(E) = (k_{Si}(E) + k_C(E))/2$ points which are obtained by averaging the values of k for Si and C components. In analogy, the bottom thick line represents the separation line between intermediate and e.r. samples and it is defined by fitting the $k_{e.r.}(E) = (k_C(E) + k_{He}(E))/2$ points which are obtained by averaging the values of k for C and He components. In the following, e.p. events will be defined as those having a k value higher than the top thick line and e.r. events those with k below the bottom thick line. The region in between, which is dominated mainly by CNO and highly contaminated by Si and He, will be defined as the intermediate sample. Such an assignment is, therefore, chosen on an event-by-event basis. Naturally, the absolute abundances of the events in the three classes depend on the location of the straight lines. For that reason, two thin lines with different slopes bracket the range of possible positions of each thick line. They represent the uncertainties in defining these energy-dependent selection cuts.

Fig. 5 shows the flux of the three components classified as previously explained. The reconstructed spectrum of the e.p. sample shows a distinct knee-like feature around 8×10^{16} eV. Applying a fit of two power laws to the spectrum with a smooth transition [13] results in a statistical significance of 3.5σ that the entire spectrum cannot be fitted with a single power law. The change of the spectral slope is $\Delta\gamma$ = -0.48 from γ = -2.76 $\pm$ 0.02 to γ = -3.24 $\pm$ 0.05 with the break position at $\log_{10}$(E/eV) = 16.92 $\pm$ 0.04. Applying

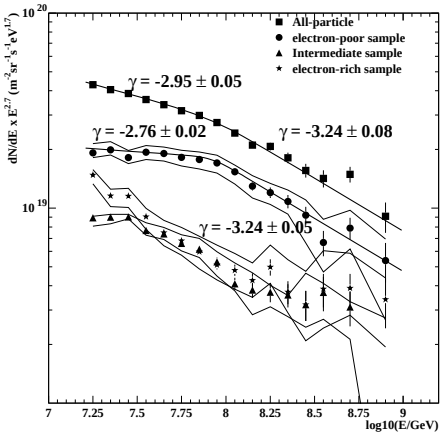

Figure 5: Reconstructed energy spectrum of the e.r., e.p. and intermediate samples as classified in the text together with the all-particle spectrum.

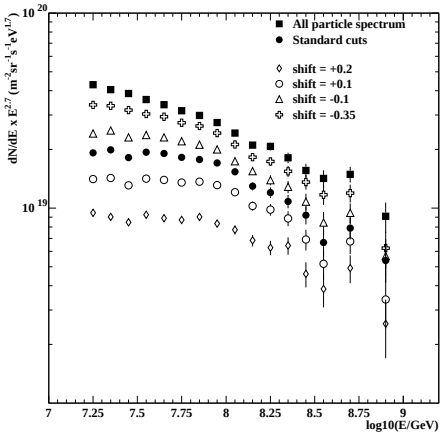

Figure 6: Effect of the shift of the cut line of the e.p. component on its energy spectrum.

the same function to the all-particle spectrum results in a statistical significance of only 2.1σ that a fit of two power laws is needed to describe the spectrum. Here the change of the spectral slope is from γ = -2.95 $\pm$ 0.05 to γ = -3.24 $\pm$ 0.08, but with the break position again at $\log_{10}$(E/eV) = 16.92 $\pm$ 0.10. The spectrum of the e.r. sample is compatible with a single power law ($\gamma \sim$ -3.37).

The error bands in the spectra show that the result is independent from the particular choice of the selection-cut lines. However, in order to further validate the present result, parallel shifts of the cut-line of the e.p. sample have been applied. Specifically, by shifting the cut line to higher values of k, the e.p. sample is enhanced, and its flux diminuishes, while shifting the cut line towards lower values of k, the e.p. sample becomes more contaminated by e.r. events and the flux increases. Fig. 6 indicates that shifting up the line cut keeps the knee-like structure unchanged, while shifts down tend to smooth out the structure. This result confirms that the structure seen in the spectrum is caused by the e.p. component, and that the conclusion is essentially independent of the particular hadronic interaction model used in the analysis.

4 Conclusions

A first result on the evolution of the k parameter, which is sensitive to the evolution of the average mass composition has been derived using an event-by-event approach, based on QGSJet II-03 model. It shows that the e.p. component shows a knee-like structure at (8.3 $\pm$ 0.8) $\times$ 10^{16} eV and the change of slope is about $\Delta\gamma \sim 0.5$ through the break. The change of slope of $\Delta\gamma \sim 0.3$ observed in the all-particle spectrum is located in the same energy range where the change of slope of the e.p. component occurs, indicating that it reflects the knee in the e.p. component. The e.r. component has a much steeper spectrum compared to the e.p. one. In the framework of the QGSJet-II-03 model, the e.p. component is the most dominant one in the energy range 10^{16} - 10^{18} eV. This result is in agreement with those obtained by other analyses of KASCADE-Grande data [14, 15, 16].

Acknowledgement: KASCADE-Grande is supported by the BMBF of Germany, the MIUR and INAF of Italy, the Polish Ministry of Science and Higher Education (this work in part by grant for 2009-2011) and the Romanian Authority for Scientific Research.

References

[1] W.-D. Apel et al. (KASCADE Collaboration), Astrop. Phys. **24** (2005) 1.
[2] M. Aglietta et al. (EAS-TOP Coll.), Astrop. Phys. **21** (2004) 583.
[3] V. Berezinsky, A. Gazizov, S. Grigorieva, Phys. Rev D **74** (2006) 043005.
[4] A.M. Hillas, J. Phys. G: Nucl. Part. Phys. **31** (2005) 95.
[5] M. Bertaina et al. (KASCADE-Grande Coll.), Proc. 31^{th} ICRC, Lodz (Poland) #icrc0323 (2009).
[6] D. Heck et al., Report FZKA 6019, Forschungszentrum Karlsruhe (1998).
[7] A. Fassò et al., Report CERN-2005-10, INFN/TC-05/11, SLAC-R-773 (2005).
[8] S.S. Ostapchenko, Nucl. Phys. B (Proc. Suppl.) **151** (2006) 143&147; S. Ostapchenko, Phys. Rev. D 74 (2006) 014026.
[9] W.-D. Apel et al. (KASCADE-Grande Collaboration), NIM A **620** (2010) 202.
[10] W.-D. Apel et al. (KASCADE Coll.), Astrop. Phys. **24** (2006) 467.
[11] A. A. Lagutin and R. I. Raikin, Nucl. Phys. Proc. Suppl., **97** (2001) 274.
[12] M. Bertaina et al. (KASCADE-Grande Collaboration), Proc. of the 22^{nd} ECRS, Turku, Finland (2010).
[13] T. Antoni et al. (KASCADE Collaboration), Astrop. Phys. **16** (2002) 245.
[14] J.-C. Arteaga, A. Chiavassa et al. (KASCADE-Grande Collaboration), this Conference Proc., #0739
[15] E. Cantoni, A. Chiavassa et al. (KASCADE-Grande Collaboration), this Conference Proc., #0504.
[16] D. Fuhrmann et al. (KASCADE-Grande Collaboration), this Conference Proc., #0280.